

## Impact of fluorinated end groups on the properties of acceptor–donor–acceptor type oligothiophenes for solution-processed photovoltaic cells†

Cite this: *J. Mater. Chem. C*, 2014, 2, 1337

Guangrui He,<sup>a</sup> Xiangjian Wan,<sup>a</sup> Zhi Li,<sup>a</sup> Qian Zhang,<sup>a</sup> Guankui Long,<sup>a</sup> Yongsheng Liu,<sup>a</sup> Yanhui Hou,<sup>b</sup> Mingtao Zhang<sup>c</sup> and Yongsheng Chen<sup>\*a</sup>

Two new oligothiophene derivatives with the acceptor–donor–acceptor structure incorporating fluorinated alkyl cyanoacetate units as the terminal acceptor groups, DCAE7T-F1 and DCAO7T-F7, have been designed and synthesized for solution-processable BHJ solar cells. The impacts of these fluorinated end groups on the optical absorption, solubility, electrochemical properties, morphology, surface energy, film forming ability, mobility and solar cell performance were studied. We found that as the fluorinated alkyl length increased, the surface energy decreased and the lipophobicity increased. Due to its high lipophobic property and a problem with its wettability, DCAO7T-F7 was not able to produce a uniform film by spin coating. A power conversion efficiency (PCE) of 2.26% was achieved with an open-circuit voltage ( $V_{oc}$ ) of 0.83 V, short circuit current ( $J_{sc}$ ) of 5.55 mA cm<sup>-2</sup> and fill factor (FF) of 0.50 for DCAE7T-F1 based solar cells. The low  $J_{sc}$  suggests that controlling the film morphology and molecular assembly is essential for the performance of these fluorinated small molecules.

Received 31st August 2013  
Accepted 11th October 2013

DOI: 10.1039/c3tc31709a

[www.rsc.org/MaterialsC](http://www.rsc.org/MaterialsC)

Over the past decade, the PCE of polymer-based bulk heterojunction organic solar cells (OPV) has been steadily increased to above 9%,<sup>1–3</sup> while that for small molecule-based bulk heterojunction (SM-BHJ) organic solar cells has been increased to over 8%.<sup>4–9</sup> In the development of organic solar cells, the rational design of a narrow band gap donor to better match the solar spectrum is one of the most successful strategies. At the same time, the morphology control of the bulk heterojunction (BHJ) active layer plays a key role in charge generation, separation and transport within the device, and finally in its overall performance.<sup>10–12</sup> The ideal morphology is a continuous interpenetrating network of donor–acceptor (D–A) components that enable easy charge transport to the electrodes. Furthermore, the D–A domains in the photoactive layer should be in a proper range (10–20 nm) to enable efficient exciton diffusion and charge separation at the D–A interface.<sup>13,14</sup> The morphology of the photoactive layer can be controlled in many ways such as

selection of the solvent, the ratio of D–A, solvent evaporation rate, the use of additives and thermal/solvent annealing.<sup>15–23</sup> In particular, the physical interaction between the donor and acceptor is the primary determinant of phase separation in the active layer.

Recently, a few reports have shown that incorporating fluorinated groups at the end of P3HT improved the device performance by improving the morphology.<sup>24–28</sup> Cho *et al.* believed that the higher PCE of the modified P3HT-based device was due to better intermixing and smaller domain sizes in the active layer, caused by a lower surface energy of the modified P3HT that is closer to that of PCBM.<sup>26,27</sup> On the other hand, Kim argued that lipophobic end-functionalized P3HT leads to larger PCBM-rich domains while maintaining P3HT crystallinity, resulting in better percolation pathways for charge transport.<sup>25</sup> The work by the Sauvé group showed that the fluorinated alkyl end group can be detrimental to the polymer solar cell device performance.<sup>28</sup> However, due to synthesis difficulties in controlling the end group composition and the molecular weight of the polymers, little work has been done to explain how the fluorinated end group impacts the performance of organic solar cells.

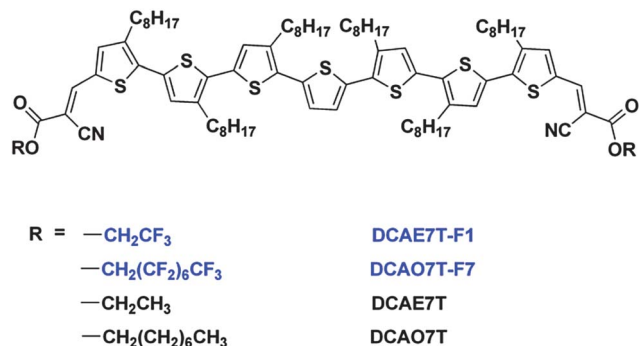
Combining the advantages of high purity, well-defined structure and molecular weight, and no batch to batch variations, small molecules could be a better platform than polymers to investigate the correlation between functional-group modification with both the active-layer morphology and the performance of the photovoltaic devices.<sup>5,12,29–36</sup> Previously, we have reported a series of small molecules using oligothiophene as

<sup>a</sup>Key Laboratory for Functional Polymer Materials and Centre for Nanoscale Science and Technology, Institute of Polymer Chemistry, College of Chemistry, Nankai University, Tianjin 300071, China. E-mail: yschen99@nankai.edu.cn; Fax: +86-(22)-2349-9992

<sup>b</sup>School of Materials Science and Engineering, Tianjin Polytechnic University, Tianjin 300160, China

<sup>c</sup>Computational Center for Molecular Science, Nankai University, Tianjin 300071, China

† Electronic supplementary information (ESI) available: <sup>1</sup>HNMR, <sup>19</sup>FNMR, <sup>13</sup>CNMR, MS, EQE, discussion of purity check of donors and other details. See DOI: 10.1039/c3tc31709a



Scheme 1 The chemical structures of DCAE7T, DCAO7T, DCAE7T-F1 and DCAO7T-F7.

the backbone and with different end groups.<sup>37–40</sup> In those studies, we find that the end groups have a great impact on the properties of oligothiophene, such as solubility, absorption, stacking and so on. Here, we report two molecules with fluorinated end groups, DCAE7T-F1 and DCAO7T-F7, and investigate the impact of fluorinated alkyl end groups on the morphology and performance of organic solar cells.

The molecular structures of DCAE7T-F1 and DCAO7T-F7 together with the counterpart molecules DCAE7T and DCAO7T<sup>37</sup> are shown in Scheme 1. First, it is found that as the fluorinated alkyl length increased, the surface energy decreased and the lipophobicity increased. For compound DCAO7T-F7 with high lipophobicity, no uniform film could be formed by spin coating. While for DCAE7T-F1, a PCE of 2.26% was achieved with a  $V_{oc}$  of 0.83 V,  $J_{sc}$  of  $5.55 \text{ mA cm}^{-2}$  and a FF of 0.50 for its SM-BHJ device. The relatively low  $J_{sc}$  is believed to be due to the poor morphology and large domains. The large domains could be explained by the aggregation of the donor caused by the fluorinated end groups.

## Experimental section

### Materials

All reactions and manipulations were carried out under an argon atmosphere using standard Schlenk techniques. All starting materials, unless otherwise specified, were purchased from commercial suppliers and used without further purification. Diformylseptithiophene (DF7T) (5,5'-diformyl-3,3',3''',3''''',3''''''-sexioctyl-2,5':2',5'':2'',2''':5''',2''''':5''''',2''''''':5''''''-septithiophene) was prepared according to the literature.<sup>41</sup> 2,2,2-Trifluoroethyl-2-cyanoacetate (CAE-F1) and 2,2,3,3,4,4,5,5,6,6,7,7,8,8,8-pentadecafluorooctyl-2-cyanoacetate (CAO-F7) were obtained by procedures similar to those reported in ref. 42–44.

### Instruments and measurements

Nuclear magnetic resonance (NMR) spectra were recorded on a Bruker AV400 Spectrometer. MALDI-TOF spectra were obtained using a Bruker Autoflex III instrument. The thermogravimetric analyses (TGA) were carried out on a NETZSCH STA 409PC instrument under nitrogen gas flow at a  $10 \text{ }^\circ\text{C min}^{-1}$  heating rate. UV-vis spectra were obtained with a JASCO V-570

spectrophotometer. The organic molecular films on quartz used for absorption spectral measurement were prepared by spin-coating their chloroform solutions. X-Ray diffraction (XRD) experiments were performed on a Rigaku D/max-2500 X-ray diffractometer with Cu-K $\alpha$  radiation ( $k = 1.5406 \text{ \AA}$ ) at 40 kV and 100 mA. Cyclic voltammetry (CV) experiments were performed with a LK98B II microcomputer-based electrochemical analyzer in  $\text{CH}_2\text{Cl}_2$  solutions. All measurements were carried out at room temperature with a conventional three-electrode configuration using a glassy carbon electrode as the working electrode, a saturated calomel electrode (SCE) as the reference electrode, and a Pt wire as the counter electrode. Dichloromethane was distilled from calcium hydride under dry nitrogen immediately prior to use. Tetrabutylammonium phosphorus hexafluoride ( $\text{Bu}_4\text{NPF}_6$ , 0.1 M) in dichloromethane was used as the supporting electrolyte, and the scan rate was  $100 \text{ mV s}^{-1}$ .

Hole mobility was measured using a similar method described in the literature,<sup>14,45</sup> with a diode configuration of ITO/PEDOT:PSS/DCAE7T-F1/Al by measuring dark current in the range of 0–8 V and fitting the results to a space charge limited form, where the space charge limited current (SCLC) is described by

$$J = 9\epsilon_0\epsilon_r\mu_h V^2/8L^3$$

where  $J$  is the current density,  $L$  is the film thickness of the active layer,  $\mu_h$  is the hole mobility,  $\epsilon_r$  is the relative dielectric constant of the transport medium,  $\epsilon_0$  is the permittivity of free space ( $8.85 \times 10^{-12} \text{ F m}^{-1}$ ),  $V$  is the internal voltage in the device and  $V = V_{\text{appl}} - V_r - V_{\text{bi}}$ , where  $V_{\text{appl}}$  is the voltage applied to the device,  $V_r$  is the voltage drop due to contact resistance and series resistance across the electrodes, and  $V_{\text{bi}}$  is the built-in voltage due to the relative work function difference of the two electrodes.

For measurements of contact angles, films of DCAE7T, DCAO7T and DCAE7T-F1 were fabricated by spin coating using an  $8 \text{ mg mL}^{-1}$  solution, while the DCAO7T-F7 film was formed by the drop method. The contact angle measurements were carried out on an Image Analysis Goniometer using a static sessile drop method.

X-ray photoelectron spectroscopy (XPS) measurements were carried out on a Kratos Axis Ultra DLD multi-technique X-ray photoelectron spectrometer.

### Fabrication and characterization of organic solar cells

The photovoltaic devices were fabricated with a structure of glass/ITO/PEDOT:PSS/donor:acceptor/LiF or Ca/Al. The ITO-coated glass substrates were cleaned by ultrasonic treatment in detergent, deionized water, acetone, and isopropyl alcohol under ultrasonication for 15 minutes each and subsequently dried by blowing nitrogen. A thin layer of PEDOT:PSS (Baytron P VP AI 4083, filtered at  $0.45 \text{ }\mu\text{m}$ ) was spin-coated (4000 rpm, ca. 40 nm thick) onto an ITO surface. After baking at  $150 \text{ }^\circ\text{C}$  for 20 min, the substrates were transferred to an argon-filled glovebox. Subsequently, an active layer was spin-coated from different blend ratios (weight-to-weight) of donor ( $8 \text{ mg mL}^{-1}$ ) and  $\text{PC}_{61}\text{BM}$  in a chloroform solution at 1500 rpm for 20 s on

the ITO/PEDOT:PSS substrate without further special treatment. The active layer thickness was measured using a Dektak 150 profilometer. Finally, a  $\sim 1$  nm LiF or 20 nm Ca layer and 80 nm Al layer were deposited on the active layer under high vacuum ( $< 3 \times 10^{-4}$  Pa). The effective area of each cell was 4 mm<sup>2</sup> defined by masks for all the solar cell devices discussed in this work.

The current density–voltage ( $J$ – $V$ ) curves of photovoltaic devices were obtained using a Keithley 2400 source-measure unit. The photocurrent was measured under simulated illumination of 100 mW cm<sup>-2</sup> AM1.5G irradiation using a xenon-lamp-based solar simulator (Oriol 96000) in an argon filled glovebox. The simulator irradiance was calibrated using a certified silicon diode.

## Synthesis

The synthesis routes towards DCAE7T-F1 and DCAO7T-F7 are shown in Scheme 2.

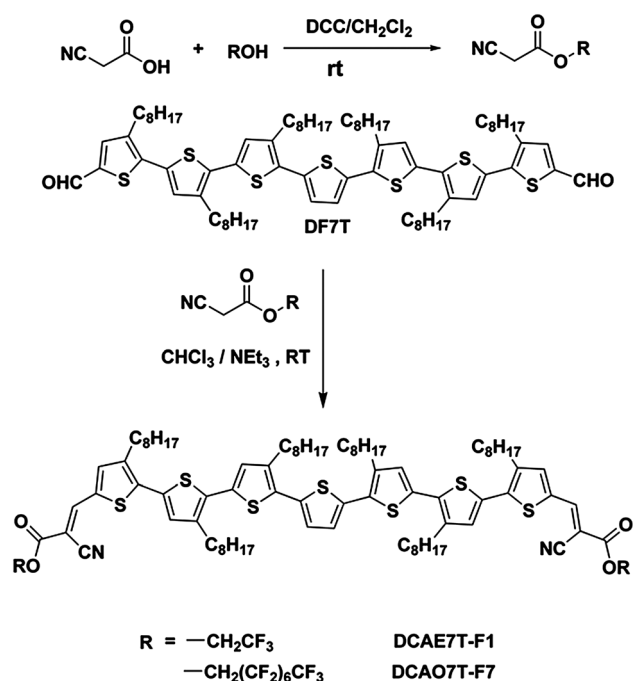
**2,2,2-Trifluoroethyl-2-cyanoacetate (CAE-F1).** To a cooled (0 °C) mixture of cyanoacetic acid (851 mg, 10 mmol) and 2,2,2-trifluoroethanol (1.05 g, 10.5 mmol) in CH<sub>2</sub>Cl<sub>2</sub> (20 mL) were successively added 1,3-dicyclohexylcarbodiimide (DCC) (2.27 g, 11 mmol) and three drops of 4-dimethylaminopyridine (DMAP). After stirring overnight at room temperature, the precipitate of urea was filtered. The filtrate was evaporated, and the residue was purified by silica gel with ethyl acetate/petroleum ether (1/4) to afford the desired compound CAE-F1 as a white solid (1.34 g, 80% yield). <sup>1</sup>H NMR (400 MHz, CDCl<sub>3</sub>):  $\delta$  4.595 (q,  $J$  = 8.0, 2H), 3.614 (s, 2H).

**2,2,3,3,4,4,5,5,6,6,7,7,8,8,8-Pentadecafluorooctyl-2-cyanoacetate (CAO-F7).** To a cooled (0 °C) mixture of cyanoacetic acid (851 mg,

10 mmol) and 2,2,3,3,4,4,5,5,6,6,7,7,8,8,8-pentadecafluorooctan-1-ol (4.20 g, 10.5 mmol) in CH<sub>2</sub>Cl<sub>2</sub> (20 mL) were successively added 1,3-dicyclohexylcarbodiimide (DCC) (2.27 g, 11 mmol) and three drops of 4-dimethylaminopyridine (DMAP). After stirring overnight at room temperature, the precipitate of urea was filtered. The filtrate was evaporated, and the residue was purified by silica gel with ethyl acetate/petroleum ether (1/6) to afford the desired compound CAO-F7 as a white solid (3.97 g, 85% yield). <sup>1</sup>H NMR (400 MHz, CDCl<sub>3</sub>):  $\delta$  4.724 (t,  $J$  = 13.2, 2H), 3.692 (s, 2H).

**DCAE7T-F1.** Diformylsepthiophene (DF7T) (130 mg, 0.10 mmol) was dissolved in a solution of dry CHCl<sub>3</sub> (50 mL). Then CAE-F1 (167 mg, 1.00 mmol) and three drops of triethylamine were added and the resulting solution was stirred for 20 hours, under argon, at room temperature. After removal of the solvent, the crude product was dissolved in 8 mL of chloroform, then precipitated from ethyl acetate and the precipitate was filtered. This procedure was repeated several times to completely remove CAE-F1. Then, the product was subjected to chromatography on silica gel using a mixture of dichloromethane and petroleum ether (1 : 2) as an eluant to produce DCAE7T-F1 as a dark green solid (118 mg, 74% yield). <sup>1</sup>H NMR (400 MHz, CDCl<sub>3</sub>):  $\delta$  8.217 (s, 2H), 7.574 (s, 2H), 7.195 (s, 2H), 7.104 (s, 2H), 7.021 (s, 2H), 4.663 (q,  $J$  = 8.0, 4H), 2.811 (m, 12H), 1.696 (m, 12H), 1.428 (m, 12H), 1.200–1.400 (m, 48H), 0.886 (m, 18H). <sup>19</sup>F NMR (400 MHz, CDCl<sub>3</sub>):  $\delta$  -73.544. <sup>13</sup>C NMR (100 MHz, CDCl<sub>3</sub>):  $\delta$  161.873, 147.439, 143.783, 142.440, 140.529, 140.184, 135.726, 134.011, 133.101, 132.301, 131.966, 131.303, 131.241, 129.233, 126.826, 126.103, 124.068, 121.311, 118.552, 115.335, 94.851, 61.934, 61.565, 61.195, 60.825, 31.954, 31.911, 30.642, 30.546, 30.033, 29.724, 29.701, 29.546, 29.472, 29.435, 29.388, 29.377, 29.320, 22.734, 14.149. MS (MALDI-FTMS)  $m/z$ : calcd for C<sub>88</sub>H<sub>116</sub>F<sub>6</sub>N<sub>2</sub>O<sub>4</sub>S<sub>7</sub> [M]<sup>+</sup>, 1602.6884; found, 1602.6875.

**DCAO7T-F7.** Diformylsepthiophene (DF7T) (130 mg, 0.10 mmol) was dissolved in a solution of dry CHCl<sub>3</sub> (50 mL). Then CAO-F7 (467 mg, 1.00 mmol) and three drops of triethylamine were added and the resulting solution was stirred for 20 hours under argon, at room temperature. After removal of the solvent, the crude product was dissolved in 8 mL of chloroform, then precipitated from ethyl acetate and the precipitate was filtered. This procedure was repeated several times to completely remove CAO-F7. Then, the product was subjected to chromatography on silica gel using a mixture of dichloromethane and petroleum ether (1 : 3) as eluant to produce DCAO7T-F7 as a dark green solid (154 mg, 70% yield). <sup>1</sup>H NMR (400 MHz, CDCl<sub>3</sub>):  $\delta$  8.229 (s, 2H), 7.600 (s, 2H), 7.216 (s, 2H), 7.111 (s, 2H), 7.031 (s, 2H), 4.800 (q,  $J$  = 12.8, 4H), 2.832 (m, 12H), 1.700 (m, 12H), 1.431 (m, 12H), 1.200–1.406 (m, 48H), 0.883 (m, 18H). <sup>19</sup>F NMR (400 MHz, CDCl<sub>3</sub>):  $\delta$  -80.793 (3F), -119.318 (2F), -121.923 (4F), -122.710 (2F), -123.200 (2F), -126.118 (2F). <sup>13</sup>C NMR (100 MHz, CDCl<sub>3</sub>):  $\delta$ : 161.929, 147.482, 143.853, 142.350, 140.637, 140.548, 140.253, 135.750, 134.002, 133.125, 132.359, 131.976, 131.297, 129.303, 126.190, 115.178, 94.916, 60.603, 31.917, 30.627, 30.541, 30.062, 29.662, 29.505, 29.430, 29.383, 29.337, 29.265, 22.690, 14.091. MS (MALDI-FTMS)  $m/z$ : calcd for C<sub>100</sub>H<sub>116</sub>F<sub>30</sub>N<sub>2</sub>O<sub>4</sub>S<sub>7</sub> [M]<sup>+</sup>, 2202.6501; found, 2202.6513.



Scheme 2 Synthesis routes towards the compounds: (I) DCC, CH<sub>2</sub>Cl<sub>2</sub>, room temperature; (II) CHCl<sub>3</sub>, triethylamine, Ar, room temperature.

## Results and discussion

### Synthesis and thermal stability of the compounds

DCAE7T-F1 and DCAO7T-F7 were synthesized by the routes shown in Scheme 2. They were obtained by the Knoevenagel reaction by directly treating their corresponding acceptor unit precursors CAE-F1 and CAO-F7 with the aldehyde-bearing precursor DF7T in the presence of triethylamine or pyridine (Scheme 2). Thermogravimetric analysis (TGA) suggests that DCAE7T-F1 and DCAO7T-F7 exhibit good stability with a decomposition temperature ( $T_d$ ) greater than 380 °C under a  $N_2$  atmosphere (see Fig. 1). Oligothiophene with a fluorinated end group exhibited high thermal stability.

### Optical absorption

The UV-vis absorption spectra of DCAE7T-F1 and DCAO7T-F7 in a dilute chloroform solution with a concentration of  $10^{-5}$  mol  $L^{-1}$  and on solid films prepared by spin coating are shown in Fig. 2. The important optical absorption data of these two new molecules, compared with those of DCAE7T and DCAO7T, are summarized in Table 1.

Compared with the absorption peaks at 492 nm of DCAE7T and DCAO7T solutions, as shown in Fig. 2a, DCAE7T-F1 (512 nm) and DCAO7T-F7 (512 nm) exhibit a red-shift of about 20 nm. In addition, the absorption coefficient of DCAE7T-F1 ( $49 L g^{-1} cm^{-1}$ ) in  $CHCl_3$  is a little higher than that of DCAE7T ( $43 L g^{-1} cm^{-1}$ ) and DCAO7T ( $40 L g^{-1} cm^{-1}$ ), while DCAO7T-F7 has a much smaller absorption coefficient ( $35 L g^{-1} cm^{-1}$ ).

In addition, as shown in Fig. 2b, the DCAE7T-F1 film, which shows a broad absorption from 350 to 760 nm, displays a red-shifted  $\lambda_{max}$  at 610 nm. DCAO7T-F7 exhibits a red-shifted absorption peak at 570 nm without a vibronic shoulder peak. The optical band gaps of DCAE7T-F1 and DCAO7T-F7 thin films were estimated from the onset of the film absorption spectra to be 1.63 eV and 1.66 eV (Table 1), lower than those of the compounds to which they are compared, DCAE7T and DCAO7T (1.72 eV).

Compared with the solution absorption, a DCAE7T-F1 film exhibits a large red-shift of about 98 nm, similar to those of

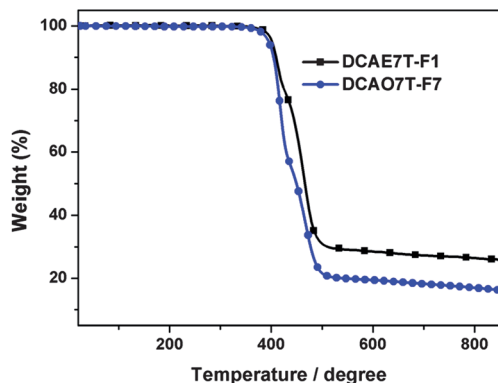


Fig. 1 TGA plot of DCAE7T-F1 and DCAO7T-F7.

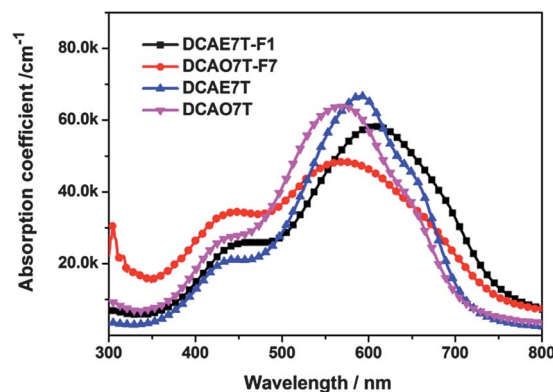
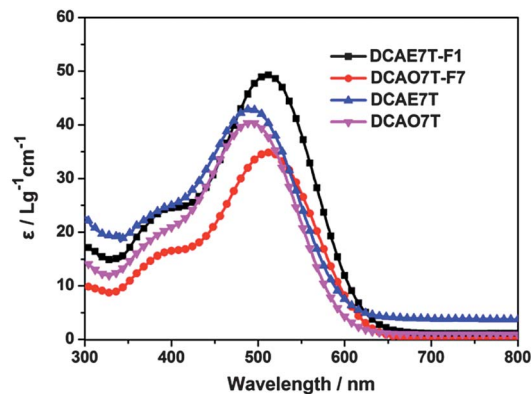


Fig. 2 (a) Absorption spectra of DCAE7T-F1, DCAO7T-F7, DCAE7T and DCAO7T in a chloroform solution; (b) absorption spectra of DCAE7T-F1, DCAO7T-F7, DCAE7T and DCAO7T as films.

DCAE7T and DCAO7T. In contrast, a DCAO7T-F7 film exhibits a much smaller red-shift (58 nm), without a vibronic shoulder peak.

### Electrochemical properties and electronic energy levels

The electrochemical properties of DCAE7T-F1 and DCAO7T-F7 were investigated by cyclic voltammetry (CV). The potentials were internally calibrated using ferrocene ( $FeCp_2$ ), assuming the absolute energy level of  $FeCp_2^{+/0}$  to be 4.8 eV below vacuum. As shown in Fig. 3, DCAE7T-F1 and DCAO7T-F7 have the same HOMO ( $-5.11$  eV) and LUMO ( $-3.44$  eV) energy levels which were calculated from the onset oxidation and reduction potentials. The electrochemical band gaps of DCAE7T-F1 and DCAO7T-F7 are estimated to be 1.67 eV. The values of the band gaps, HOMO and LUMO energy levels of the two compounds, along with those of DCAE7T and DCAO7T molecules for comparison, are listed in Table 1 from which we can see that the HOMO energy levels of these molecules are very similar ( $-5.11$  to  $-5.13$  eV), which is predominantly determined by the donor moiety (oligothiophene unit). Different from the HOMO energy levels, the LUMO energy levels of these molecules changed distinctly, leading to different band gaps for these molecules, from 1.84 eV to 1.67 eV.

These results are consistent with those from optical data and demonstrate that the band gap of these kinds of molecules can be tuned effectively through introduction of a different acceptor terminal unit.

Table 1 Optical and electrochemical data for the molecules DCAE7T-F1, DCAO7T-F7, DCAE7T and DCAO7T

Compounds	$\lambda_{\max}$ solution (nm)	$\epsilon$ solution ( $L g^{-1} cm^{-1}$ )	$\lambda_{\max}$ film (nm)	$(E_g^{opt})$ film (eV)	$E_g^{cv}$ (eV)	HOMO (eV)	LUMO (eV)
DCAE7T-F1	512	49	610	1.63	1.67	-5.11	-3.44
DCAO7T-F7	512	35	570	1.66	1.67	-5.11	-3.44
DCAE7T <sup>a</sup>	492	43	591	1.72	1.83	-5.13	-3.30
DCAO7T <sup>a</sup>	492	40	580	1.74	1.84	-5.13	-3.29

<sup>a</sup> Data from ref. 37 and  $\epsilon$  solution data from ref. 40.

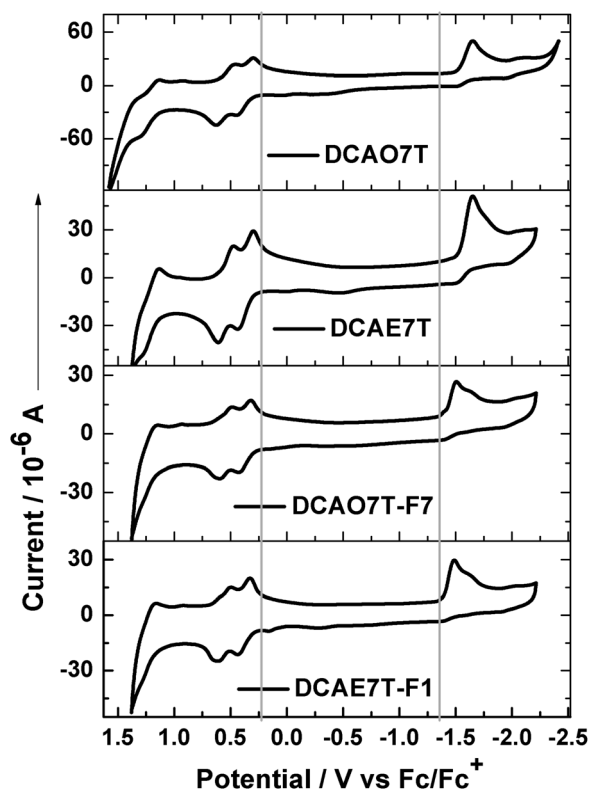


Fig. 3 Cyclic voltammograms of DCAE7T-F1 and DCAO7T-F7 solutions on a Pd/C electrode in a dichloromethane solution of  $0.1 \text{ mol L}^{-1} \text{ Bu}_4\text{NPF}_6$  at a scan rate of  $100 \text{ mV s}^{-1}$ .

#### X-ray diffraction (XRD) and structure calculation

The structural order of pristine DCAE7T-F1, DCAO7T-F7, DCAE7T and DCAO7T was investigated by X-ray diffraction (XRD) analysis for the films of DCAE7T-F1, DCAE7T and DCAO7T spin-coated from  $\text{CHCl}_3$  solutions onto glass substrates and the films of DCAO7T-F7 dropped onto a glass substrate. The XRD patterns of DCAE7T-F1, DCAO7T-F7, DCAE7T and DCAO7T films are shown in Fig. 4.

It can be seen that all these four molecular films exhibited strong diffraction peaks (100), corresponding to the  $d_{100}$ -spacing which is the distance between the planes of the main conjugation chains of these molecules. The second and third order diffraction peaks, (200) and (300), are also observed.

To give a rough estimation of the crystallinities of the new molecules, DCAE7T-F1 and DCAO7T-F7, compared to those of

DCAE7T and DCAO7T, we chose the diffraction peak corresponding to the (100) orientation of the organic crystallite to study. In addition, the films of DCAE7T-F1, DCAE7T and DCAO7T have a similar film thickness. From Fig. 4, it can be seen that the intensity of the diffraction peak increased substantially from DCAE7T-F1 to DCAE7T and DCAO7T, while the DCAO7T-F7 film shows a significantly weak diffraction peak. The above results indicate that the fluorinated end group, to some extent, decreased the crystallinity of the molecules DCAO7T-F7 and DCAE7T-F1 in the films.

#### Hole mobility

The hole mobility of the pristine DCAE7T-F1 film was measured by the SCLC method. Comparing with the polymer

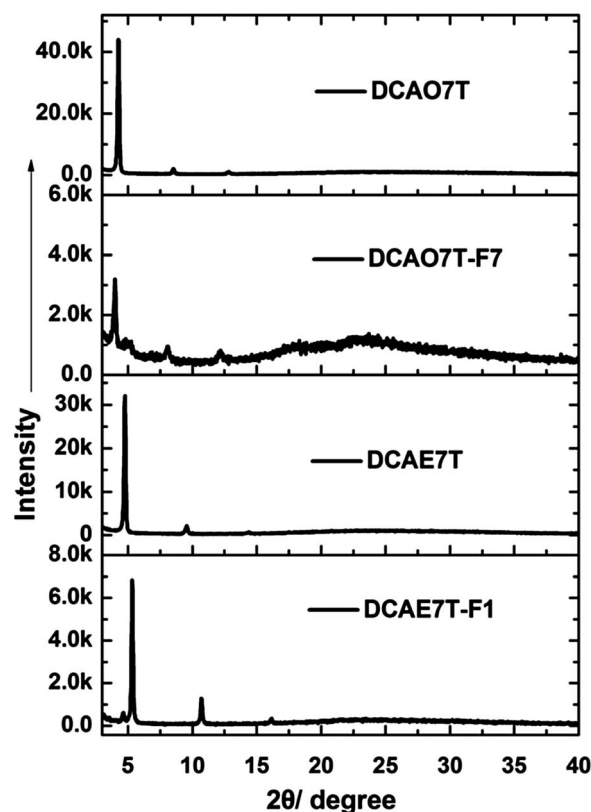


Fig. 4 XRD patterns of DCAO7T, DCAE7T and DCAE7T-F1 films spin-coated from  $\text{CHCl}_3$  onto a glass substrate. The DCAO7T-F7 film was drop onto the glass substrate.

counterparts, small molecules have a definite structure, therefore high purity and less batch to batch variations. Thus there are lower traps, recombination or defect centres in the small molecule based devices, which is the primary reason that we used the trap-free model to fit the data. As plotted in Fig. S6,† the hole mobility of the DCAE7T-F1 film is  $0.77 \times 10^{-4} \text{ cm}^2 \text{ V}^{-1} \text{ s}^{-1}$ , lower than that of DCAE7T ( $4.51 \times 10^{-4} \text{ cm}^2 \text{ V}^{-1} \text{ s}^{-1}$ ) and DCAO7T ( $3.26 \times 10^{-4} \text{ cm}^2 \text{ V}^{-1} \text{ s}^{-1}$ ).<sup>37</sup> The hole mobility results can be explained by the above XRD data. The hole mobility of the DCAO7T-F7 film could not be tested because it cannot be made by spin coating, as discussed below.

### Film formation and surface energy test

For the fabrication of films, spin-coating is a preferred technique as it is simple, consistent, and allows for small-scale production.<sup>46,47</sup> Here, we investigated the film forming abilities of DCAE7T-F1 and DCAO7T-F7, together with those of DCAE7T and DCAO7T. Solutions of DCAE7T-F1, DCAO7T-F7, DCAE7T and DCAO7T with a concentration of  $8 \text{ mg mL}^{-1}$  were prepared. The solutions were dropped onto cleaned ITO substrates and spin coated to form a film. As shown in Fig. 5, from 1(a) to 1(d), it can be seen that DCAE7T-F1, DCAE7T and DCAO7T form good films by the spin coating method, while DCAO7T-F7 does not form a uniform film with good quality.

The wettability of the substrate by the polymer solution is generally used for spin coating, and is important for the spreading of the dispensed drop and finally the uniform film formation with the aid of centrifugal forces.<sup>47</sup> We then investigated the difference in the wettability of the solutions on the ITO substrate. We dropped each of the four solutions onto ITO substrates and allowed them to dry and then checked the spreading of similar sized  $\text{CHCl}_3$  droplets dispersed onto ITO. As shown in Fig. 5, from 2(a) to 2(d), we found that the solutions of DCAE7T-F1, DCAE7T and DCAO7T did not spread out, while the DCAO7T-F7 solution condensed to one dot. From Fig. S7,† it can be seen that when the DCAO7T-F7 solution was dropped onto the ITO surface, the drop keeps at a certain contact angle ( $13.8^\circ$ ) before drying, while the other oligothiophene derivative showed perfect spreading with no measurable angle.

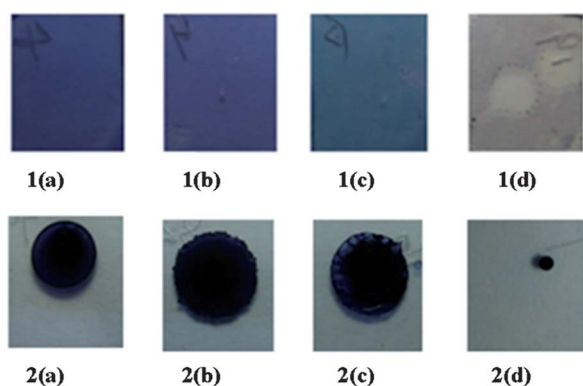


Fig. 5 Images of films produced by spin-coating: 1(a) DCAE7T, 1(b) DCAO7T, 1(c) DCAE7T-F1, and 1(d) DCAO7T-F7 ( $\sim 1.7 \text{ cm} \times 1.8 \text{ cm}$ ); images of films when produced by drop coating: 2(a) DCAE7T, 2(b) DCAO7T, 2(c) DCAE7T-F1, and 2(d) DCAO7T-F7 ( $\sim 1.7 \text{ cm} \times 1.8 \text{ cm}$ ).

In order to further investigate the above phenomena, contact angle measurements were carried out on an image analysis goniometer using a static sessile drop method.  $0.5 \mu\text{L}$  droplets of (i) water, (ii) glycol, and (iii) diiodomethane were placed on a substrate of one of the oligothiophene films and imaged. The corresponding surface energies were calculated (the calculation process of the surface energy can be seen in the ESI†)<sup>48,49</sup> and are given in Table 2. As shown in Table 2, it can be seen that, along with the increase of the size of fluorinated alkylcyanoacetate, the surface free energy decreased. The contact angle of  $\text{CH}_2\text{I}_2$  increased from DCAO7T ( $10.02^\circ$ ) and DCAE7T ( $14.64^\circ$ ), to DCAE7T-F1 ( $19.00^\circ$ ) and DCAO7T-F7 ( $28.88^\circ$ ), while the contact angles of water and glycol on these four molecular films were very similar. From the above test, it can be seen that when a larger amount of fluorine was introduced into the oligothiophene backbone, the material became more lipophobic, with a smaller surface free energy. The high lipophobicity of DCAO7T-F7 prevents it from forming a film by spin-coating.

### Photovoltaic performance

BHJ organic solar cells were fabricated using the new molecule DCAE7T-F1 as the donor material, and  $\text{PC}_{61}\text{BM}$  as the acceptor material, using the conventional solution spin-coating process. The device structure is ITO/PEDOT:PSS/photoactive layer/LiF/Al. Device optimization was conducted by changing the weight ratios of the donor vs. acceptor (summarized in Tables 3 and 4 and shown in Fig. 6 and 7). The best typical current density–voltage ( $J$ - $V$ ) curves of the SM BHJs are shown in Fig. 6 and the results are summarized in Table 3. For DCAO7T-F7, its high lipophobicity prevents its use in SM BHJ devices.

For DCAE7T-F1, the best efficiency was obtained from the device with the active layer comprised of a blend of DCAE7T-F1 and  $\text{PC}_{61}\text{BM}$  with a weight ratio of 1 : 0.5 and an optimized thickness of about 90 nm, using LiF/Al as the cathode. This SM-BHJ device gave a  $V_{\text{oc}}$  of 0.83 V,  $J_{\text{sc}}$  of  $5.50 \text{ mA cm}^{-2}$ , a FF of 0.50 and a PCE of 2.26%.

Compared with the performance of DCAE7T and DCAO7T based organic solar cells (Table 4), it is found that DCAE7T-F1 based SM-BHJ devices showed a much lower  $J_{\text{sc}}$ . The result can be explained by the TEM results. As shown in Fig. 7, a rather large domain size (50–60 nm) was found for this material in the active layer, which might be driven by the aggregation of the fluorinated end groups.<sup>50,51</sup>

During the optimization of DCAE7T-F1 based SM-OPV devices, we found significant inhomogeneity of the device performance on the same ITO substrates with five parallel separated devices (Table S2†). From Fig. S8,† it can be seen that the outside devices show good performance (PCE = 2.26%), while the middle device shows the worst performance (PCE = 0.85%). In order to understand this, we carried out XPS analysis. From Table S3† we can see that there is a significant change in the peak intensity corresponding to fluorine atoms between the edge and middle positions in the ITO substrate. From the AFM images (Fig. 8) of these blend active films, we can see that there is a large variation of morphology in the film of DCAE7T-F1/

Table 2 Contact angle data of test liquids on the surface of oligothiophene films and surface energy data of the films

	DCAE7T	DCAO7T	DCAE7T-F1	DCAO7T-F7
Contact angle H <sub>2</sub> O	93.60°	103.01°	97.84°	101.14°
Contact angle HOCH <sub>2</sub> CH <sub>2</sub> OH	74.12°	77.03°	82.16°	80.40°
Contact angle CH <sub>2</sub> I <sub>2</sub>	14.64°	10.02°	19.00°	28.88°
Surface energy (mJ m <sup>-2</sup> )	49.18	50.41	48.02	44.66

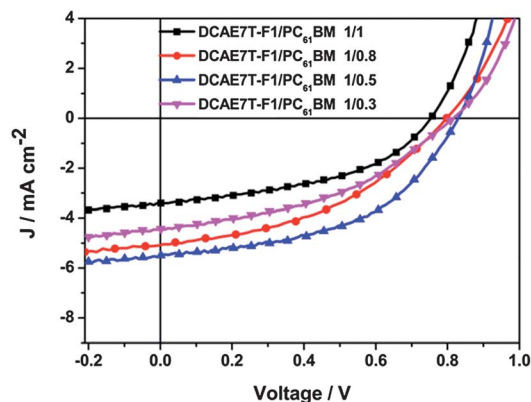
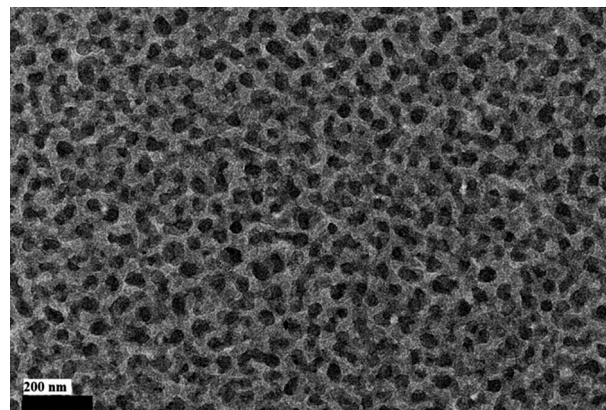
Table 3 Current density–voltage characteristics of the SM-OPV devices based on blends of DCAE7T-F1/PC<sub>61</sub>BM with different (w/w) ratios under an illumination of AM.1.5, 100 mW cm<sup>-2</sup>. The device structure is ITO/PEDOT:PSS/DCAE7T-F1:PC<sub>61</sub>BM/LiF/Al

DCAE7T-F1:PC <sub>61</sub> BM	V <sub>oc</sub> (V)	J <sub>sc</sub> (mA cm <sup>-2</sup> )	FF (%)	PCE (%)
1/0.8	0.80	5.09	0.27	1.71
1/0.5	0.83	5.50	0.50	2.26
1/0.3	0.82	4.66	0.30	1.50

PC<sub>61</sub>BM. Until now, the detailed mechanism of the phenomenon is not clear. However, we believe that this difference in the distribution of fluorine is primarily due to the tendency of the fluorinated end groups in the solution to orient differently at the solution–air interface during the film forming process, and this has a large effect on the morphology and ratio of the donor–acceptor of the final spin-coated film.<sup>51,52</sup>

Comparing our results with those reported for fluorinated end group organic solar cells,<sup>25–28</sup> it can be seen that the relative fluorine content in the molecule has a great impact on the performance of molecule based organic solar cell devices. The structures of some reported fluorinated end group polymers are shown in Scheme 3.

The fluorine content of these polymers varied from *ca.* 0.52% (PCDTBT-CF<sub>3</sub>) and 0.85% (H-P3HT-PhO(CO)C<sub>3</sub>F<sub>7</sub>), to 1.03% (H-P3HT-CF<sub>2</sub>CF<sub>3</sub>) and 2.01% (H-P3HT-CF<sub>2</sub>(CF<sub>2</sub>)<sub>2</sub>CF<sub>3</sub>), and finally to 2.81% (H-P3HT-CF<sub>2</sub>(CF<sub>2</sub>)<sub>4</sub>CF<sub>3</sub>). From the literature,<sup>25–28</sup> we can see that when the fluorine content is low, 0.52% (PCDTBT-CF<sub>3</sub>) and 0.85% (H-P3HT-PhO(CO)C<sub>3</sub>F<sub>7</sub>), these polymer based solar cells show better performance compared with the unfluorinated end group polymers. When the fluorine content increased to *ca.* 1.03% (H-P3HT-CF<sub>2</sub>CF<sub>3</sub>), 2.01% (H-P3HT-CF<sub>2</sub>(CF<sub>2</sub>)<sub>2</sub>CF<sub>3</sub>), 2.81% (H-P3HT-CF<sub>2</sub>(CF<sub>2</sub>)<sub>4</sub>CF<sub>3</sub>) and 7.11% (DCAE7T-F1), a worse performance was produced. When the fluorine content increased further, *ca.* 25.86% (DCAO7T-F7), the fluorinated end group affects the film forming ability of these molecules because of the wettability problem (Table 5).

Fig. 6 Current density–voltage characteristics of the SM BHJ devices based on blends of DCAE7T-F1/PC<sub>61</sub>BM with different (w/w) ratios under an illumination of AM.1.5, 100 mW cm<sup>-2</sup>.Fig. 7 TEM of DCAE7T-F1:PC<sub>61</sub>BM (2 : 1) film produced by spin-coating.

Now, we can give a complete description of the influence of fluorinated alkyl end groups on the properties of polymers for use in organic solar cells. Incorporation of a small amount of

Table 4 Current density–voltage characteristics of the best SM BHJ devices based on DCAE7T-F1, DCAE7T and DCAO7T under an illumination of AM.1.5, 100 mW cm<sup>-2</sup>

Active Layer	V <sub>oc</sub> /V	J <sub>sc</sub> /mA cm <sup>-2</sup>	FF	PCE (%)	μ <sub>h</sub> /cm <sup>2</sup> V <sup>-1</sup> s <sup>-1</sup> 10 <sup>-4</sup>
DCAO7T:PC <sub>61</sub> BM <sup>a</sup>	0.86	10.74	0.55	5.08	3.26
DCAE7T:PC <sub>61</sub> BM <sup>a</sup>	0.88	9.94	0.51	4.46	4.51
DCAE7T-F1:PC <sub>61</sub> BM	0.83	5.55	0.50	2.26	0.77

<sup>a</sup> Data from ref. 37.

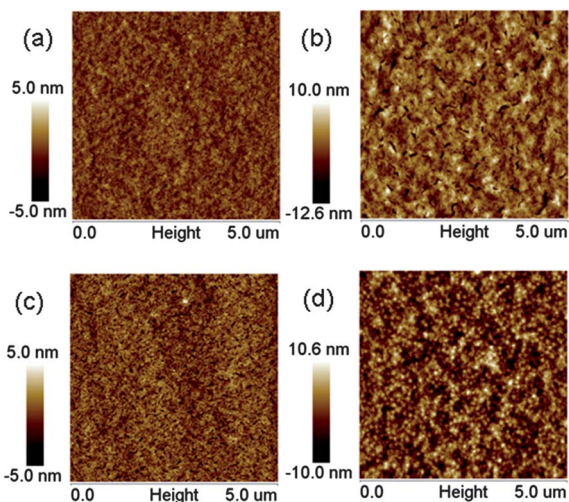
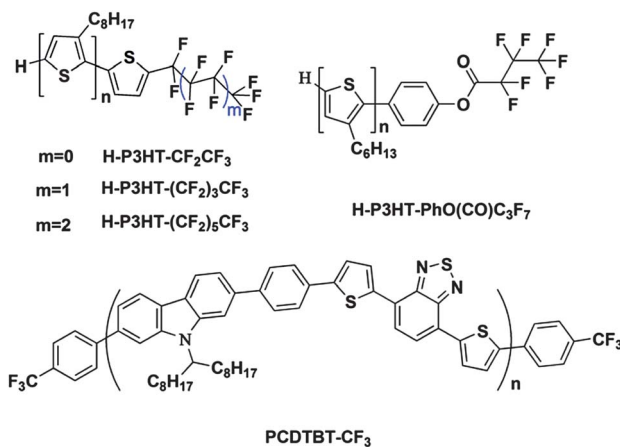


Fig. 8 Tapping-mode AFM height images ( $5 \times 5 \mu\text{m}$ ) of blend films (w/w: 1 : 0.5) spin-coated from chloroform solutions. (a) Blend film of DCAE7T/PC<sub>61</sub>BM. (b) Blend film of DCAO7T/PC<sub>61</sub>BM. (c) Blend film of DCAE7T-F1/PC<sub>61</sub>BM. (d) Blend film of DCAO7T-F7/PC<sub>61</sub>BM.



Scheme 3 Structures of several polymers with fluorinated alkyl end groups reported in the literature.

fluorine into the polymer backbone is shown to improve the device performance. When the fluorine content is low, the mismatch of the donor and acceptor will dominate, and thus a

Table 5 Data on the fluorine content of DCAE7T-F1 and DCAO7T-F7 and other reported fluorinated end group polymers and the performance of their corresponding OPV devices, compared with the unfluorinated analog (values in brackets), under an illumination of AM1.5,  $100 \text{ mW cm}^{-2}$

Compounds	Mn	PDI	F% (mass)	PCE (%)
DCAO7T-F7	2204	1.00	25.86%	NO (5.08)
DCAE7T-F1	1604	1.00	7.11%	2.26 (4.46)
H-P3HT- $\text{CF}_2(\text{CF}_2)_4\text{CF}_3^a$	8800	1.20	2.81%	0.32 (3.2)
H-P3HT- $\text{CF}_2(\text{CF}_2)_2\text{CF}_3^a$	8500	1.20	2.01%	0.63 (3.2)
H-P3HT- $\text{CF}_2\text{CF}_3^a$	9200	1.20	1.03%	1.3 (3.2)
H-P3HT-PhO(CO) $\text{C}_3\text{F}_7^b$	15 600	1.36	0.85%	4.5 (3.2)
PCDTBT- $\text{CF}_3^c$	11 000	5.44	0.52%	6.02 (4.82)

<sup>a</sup> Data from ref. 28. <sup>b</sup> Data from ref. 27. <sup>c</sup> Data from ref. 26.

smaller domain is produced. When the fluorine content is increased, the lipophobicity becomes more and more important, while the mismatch effect decreases and a large domain is formed. When the fluorine content increases further, the lipophobicity dominates and a wettability problem is produced. Concerning the molecular weight difference, the same end group is relatively more significant in small molecule donors than in polymer donors, so the end group has a larger effect on the performance of small molecule based devices.

## Summary

We have synthesized two small molecules DCAE7T-F1 and DCAO7T-F7 based on our previous compounds DCAO7T and DCAE7T by introducing fluorinated alkyl chains into the terminal unit. It has been found that fluoro substituted alkyl chains in the terminal unit have a great impact not only on the absorption energy levels but also on the film forming properties and thus the device performance. A PCE of 2.26% was achieved with a  $V_{oc}$  of 0.83 V,  $J_{sc}$  of  $5.55 \text{ mA cm}^{-2}$  and FF of 0.50 for DCAE7T-F1 based solar cells. It is noted that with the increase of fluorine atom content from DCAE7T-F1 to DCAO7T-F7, the surface energy decreased significantly, along with an increase of the lipophobic property. The large lipophobic property of DCAO7T-F7 prevents it from forming films by spin-coating. Our results demonstrate that the lipophobic property, film forming ability and structure must be considered collectively for new molecular design and synthesis.

## Acknowledgements

The authors gratefully acknowledge financial support from the MOST (Grants 2012CB933401 and 2011DFB50300), NSFC (Grants 50933003, 51273093 and 21004043), NSF of Tianjin City (Grant 10ZCGHHZ00600) and PCSIRT (IRT1257).

## Notes and references

- Z. He, C. Zhong, X. Huang, W.-Y. Wong, H. Wu, L. Chen, S. Su and Y. Cao, *Adv. Mater.*, 2011, **23**, 4636–4643.
- Z. He, C. Zhong, S. Su, M. Xu, H. Wu and Y. Cao, *Nat. Photonics*, 2012, **6**, 591–595.
- L. Dou, C.-C. Chen, K. Yoshimura, K. Ohya, W.-H. Chang, J. Gao, Y. Liu, E. Richard and Y. Yang, *Macromolecules*, 2013, **46**, 3384–3390.
- A. K. K. Kyaw, D. H. Wang, V. Gupta, J. Zhang, S. Chand, G. C. Bazan and A. J. Heeger, *Adv. Mater.*, 2013, **25**, 2397–2402.
- A. K. K. Kyaw, D. H. Wang, V. Gupta, W. L. Leong, L. Ke, G. C. Bazan and A. J. Heeger, *ACS Nano*, 2013, **7**, 4569–4577.
- J. Zhou, X. Wan, Y. Liu, Y. Zuo, Z. Li, G. He, G. Long, W. Ni, C. Li, X. Su and Y. Chen, *J. Am. Chem. Soc.*, 2012, **134**, 16345–16351.
- D. H. Wang, A. K. K. Kyaw, V. Gupta, G. C. Bazan and A. J. Heeger, *Adv. Energy Mater.*, 2013, **3**, 1161–1165.
- J. Zhou, Y. Zuo, X. Wan, G. Long, Q. Zhang, W. Ni, Y. Liu, Z. Li, G. He, C. Li, B. Kan, M. Li and Y. Chen, *J. Am. Chem. Soc.*, 2013, **135**, 8484–8487.

- 9 Y. Chen, X. Wan and G. Long, *Acc. Chem. Res.*, 2013, DOI: 10.1021/ar400088c.
- 10 B. C. Thompson and J. M. J. Fréchet, *Angew. Chem., Int. Ed.*, 2008, **47**, 58–77.
- 11 V. D. Mihailetschi, H. X. Xie, B. de Boer, L. J. A. Koster and P. W. M. Blom, *Adv. Funct. Mater.*, 2006, **16**, 699–708.
- 12 A. Mishra and P. Bäuerle, *Angew. Chem., Int. Ed.*, 2012, **51**, 2020–2067.
- 13 A. C. Mayer, S. R. Scully, B. E. Hardin, M. W. Rowell and M. D. McGehee, *Mater. Today*, 2007, **10**, 28–33.
- 14 F. He and L. Yu, *J. Phys. Chem. Lett.*, 2011, **2**, 3102–3113.
- 15 S. J. Lou, J. M. Szarko, T. Xu, L. Yu, T. J. Marks and L. X. Chen, *J. Am. Chem. Soc.*, 2011, **133**, 20661–20663.
- 16 J. K. Lee, W. L. Ma, C. J. Brabec, J. Yuen, J. S. Moon, J. Y. Kim, K. Lee, G. C. Bazan and A. J. Heeger, *J. Am. Chem. Soc.*, 2008, **130**, 3619–3623.
- 17 K. R. Graham, J. Mei, R. Stalder, J. W. Shim, H. Cheun, F. Steffy, F. So, B. Kippelen and J. R. Reynolds, *ACS Appl. Mater. Interfaces*, 2011, **3**, 1210–1215.
- 18 S. Kwon, J. K. Park, G. Kim, J. Kong, G. C. Bazan and K. Lee, *Adv. Energy Mater.*, 2012, **2**, 1413.
- 19 L. G. Kaake, G. C. Welch, D. Moses, G. C. Bazan and A. J. Heeger, *J. Phys. Chem. Lett.*, 2012, **3**, 1253–1257.
- 20 H. Zhou, Y. Zhang, J. Seiffter, S. D. Collins, C. Luo, G. C. Bazan, T.-Q. Nguyen and A. J. Heeger, *Adv. Mater.*, 2013, **25**, 1646–1652.
- 21 J. A. Love, C. M. Proctor, J. Liu, C. J. Takacs, A. Sharenko, T. S. van der Poll, A. J. Heeger, G. C. Bazan and T.-Q. Nguyen, *Adv. Funct. Mater.*, 2013, **23**, 5019–5026.
- 22 W. L. Leong, G. C. Welch, J. Seiffter, J. H. Seo, G. C. Bazan and A. J. Heeger, *Adv. Energy Mater.*, 2013, **3**, 356–363.
- 23 J. A. Carr, K. S. Nalwa, R. Mahadevapuram, Y. Chen, J. Anderegge and S. Chaudhary, *ACS Appl. Mater. Interfaces*, 2012, **4**, 2831–2835.
- 24 K. Yao, L. Chen, X. Chen and Y. Chen, *Chem. Mater.*, 2013, **25**, 897–904.
- 25 B. Lim, J. Jo, S.-I. Na, J. Kim, S.-S. Kim and D.-Y. Kim, *J. Mater. Chem.*, 2010, **20**, 10919–10923.
- 26 C. Shim, M. Kim, S.-G. Ihn, Y. S. Choi, Y. Kim and K. Cho, *Chem. Commun.*, 2012, **48**, 7206–7208.
- 27 J. S. Kim, Y. Lee, J. H. Lee, J. H. Park, J. K. Kim and K. Cho, *Adv. Mater.*, 2010, **22**, 1355–1360.
- 28 Z. Mao, K. Vakhshouri, C. Jaye, D. A. Fischer, R. Fernando, D. M. DeLongchamp, E. D. Gomez and G. Sauvé, *Macromolecules*, 2013, **46**, 103–112.
- 29 Y. Lin, Y. Li and X. Zhan, *Chem. Soc. Rev.*, 2012, **41**, 4245–4272.
- 30 S. Shen, P. Jiang, C. He, J. Zhang, P. Shen, Y. Zhang, Y. Yi, Z. Zhang, Z. Li and Y. Li, *Chem. Mater.*, 2013, **25**, 2274–2281.
- 31 D. Demeter, T. Rousseau, P. Leriche, T. Cauchy, R. Po and J. Roncali, *Adv. Funct. Mater.*, 2011, **21**, 4379–4387.
- 32 W. L. Leong, G. C. Welch, L. G. Kaake, C. J. Takacs, Y. Sun, G. C. Bazan and A. J. Heeger, *Chem. Sci.*, 2012, **3**, 2103–2109.
- 33 J. Huang, C. Zhan, X. Zhang, Y. Zhao, Z. Lu, H. Jia, B. Jiang, J. Ye, S. Zhang, A. Tang, Y. Liu, Q. Pei and J. Yao, *ACS Appl. Mater. Interfaces*, 2013, **5**, 2033–2039.
- 34 J. Zhou, X. Wan, Y. Liu, G. Long, F. Wang, Z. Li, Y. Zuo, C. Li and Y. Chen, *Chem. Mater.*, 2011, **23**, 4666–4668.
- 35 M. T. Lloyd, J. E. Anthony and G. G. Malliaras, *Mater. Today*, 2007, **10**, 34–41.
- 36 H.-Y. Lin, W.-C. Huang, Y.-C. Chen, H.-H. Chou, C.-Y. Hsu, J. T. Lin and H.-W. Lin, *Chem. Commun.*, 2012, **48**, 8913–8915.
- 37 Y. Liu, X. Wan, F. Wang, J. Zhou, G. Long, J. Tian, J. You, Y. Yang and Y. Chen, *Adv. Energy Mater.*, 2011, **1**, 771–775.
- 38 Z. Li, G. He, X. Wan, Y. Liu, J. Zhou, G. Long, Y. Zuo, M. Zhang and Y. Chen, *Adv. Energy Mater.*, 2011, **2**, 74–77.
- 39 G. He, Z. Li, X. Wan, Y. Liu, J. Zhou, G. Long, M. Zhang and Y. Chen, *J. Mater. Chem.*, 2012, **22**, 9173–9180.
- 40 G. He, Z. Li, X. Wan, J. Zhou, G. Long, S. Zhang, M. Zhang and Y. Chen, *J. Mater. Chem. A*, 2013, **1**, 1801–1809.
- 41 Y. S. Liu, J. Y. Zhou, X. J. Wan and Y. S. Chen, *Tetrahedron*, 2009, **65**, 5209–5215.
- 42 M. H. D. Postema, J. L. Piper, R. L. Betts, F. A. Valeriote and H. Pietraszkewicz, *J. Org. Chem.*, 2004, **70**, 829–836.
- 43 G. Shen and B. S. J. Blagg, *Org. Lett.*, 2005, **7**, 2157–2160.
- 44 J.-M. Vatele, *Tetrahedron Lett.*, 2005, **46**, 2299–2301.
- 45 Y. Liang, D. Feng, Y. Wu, S.-T. Tsai, G. Li, C. Ray and L. Yu, *J. Am. Chem. Soc.*, 2009, **131**, 7792–7799.
- 46 N. Sahu, B. Parija and S. Panigrahi, *Indian J. Phys.*, 2009, **83**, 493–502.
- 47 S. Roy, K. J. Ansari, S. S. K. Jampa, P. Vutukuri and R. Mukherjee, *ACS Appl. Mater. Interfaces*, 2012, **4**, 1887–1896.
- 48 C. J. Van Oss, M. K. Chaudhury and R. J. Good, *Chem. Rev.*, 1988, **88**, 927–941.
- 49 M. H. V. C. Adão, B. J. V. Saramago and A. C. Fernandes, *J. Colloid Interface Sci.*, 1999, **217**, 94–106.
- 50 D. Xue, X. Wang, H. Ni, W. Zhang and G. Xue, *Langmuir*, 2009, **25**, 2248–2257.
- 51 A. Synytska, D. Appelhans, Z. G. Wang, F. Simon, F. Lehmann, M. Stamm and K. Grundke, *Macromolecules*, 2006, **40**, 297–305.
- 52 H. Ni, X. Li, Y. Hu, B. Zuo, Z. Zhao, J. Yang, D. Yuan, X. Ye and X. Wang, *J. Phys. Chem. C*, 2012, **116**, 24151–24160.